Acta metall. mater. Vol. 39, No. 7, pp. 1571–1577, 1991
Printed in Great Britain.

0956-7151/91 $3.00 + 0.00

A STUDY OF GRAIN BOUNDARY TRANSLATIONAL STATES IN A $\Sigma 3[\bar{1}10]/(\bar{1}\bar{1}1)$ BICRYSTAL

P. A. DEYMIER, M. SHAMSUZZOHA and J. D. WEINBERG
Department of Materials Science and Engineering, University of Arizona, Tucson, AZ 85721, U.S.A.

(Received 11 October 1989; in revised form 4 December 1990)

Abstract—High-resolution electron microscopy images of a $\Sigma 3[\bar{1}10]/(\bar{1}\bar{1}1)$ bicrystal produced by heavy cold rolling and annealing show a multiplicity of grain boundary core structures. Two grain boundary states are separated by a partial grain boundary dislocation with Burgers vector $\mathbf{b} = 1/2\ \mathbf{b}_1$ (where $\mathbf{b}_1 = 1/6[112]$ is the Burgers vector of a secondary dislocation). This implies a change in translational state. All other structures are related through continuous transport of atoms from one grain to the other resulting in $[\bar{1}\bar{1}1]$ grain boundary steps. Calculations of the energy associated with the observed structures indicate that the two perfect twin states $\mathbf{t} = 0$ and $2\mathbf{b}_1$ are stable, while all other grain boundary translational states are metastable.

Résumé—Des images de microcopie électronique en haute résolution d'un bicristal $\Sigma 3\ [\bar{1}10]/(\bar{1}\bar{1}1)$ produit par laminage à froid et recuit révèlent un grand nombre de structures de coeur de joints de grains. Deux états de joints de grains sont séparés par une dislocation imparfaite de joints de grains, de vecteur de Burgers $\mathbf{b} = 1\text{–}2\mathbf{b}_1$ (où $\mathbf{b}_1 = 1/6\ [112]$ est le vecteur de Burgers d'une dislocation secondaire). Ceci implique un changement de l'état de translation. Toutes les autres structures sont reliées par un transport continu d'atomes d'un grain vers l'autre, ce qui donne des marches de joints de grains $[\bar{1}\bar{1}1]$. Des calculs de l'énergie associée aux structures observées indiquent que les deux états de macle parfaite $\mathbf{t} = 0$ et $2\mathbf{b}_1$ sont stables, tandis que tous les autres états de translation des joints de grains sont métastables.

Zusammenfassung—Hochaufgelöste elektronenmikroskopische Durchstrahlungsbilder eines $\Sigma = 3[110/(111)$-Bikristalles, hergestellt durch starkes Walzen und Ausheilen, weisen auf eine Anzahl von korngrenzstrukturen hin. Zwei verschiedene Korngrenzzustände werden voneinander getrennt durch eine Teil-Korngrenzversetzung mit Burgersvektor $\mathbf{b} = 1/2\ \mathbf{b}_1$ (wobei $\mathbf{b}_1 = 1/6[112]$ der Burgersvektor einer sekundären Versetzung ist). Das bedeutet ein Wechsel im Translationszustand. Alle anderen Strukturen hängen über kontinuierlichen Transport von Atomen von einem Korn zum anderen, welches zu [111]-Korngrenzstufen führt, zusammen. Berechnungen der mit den beobachteten Strukturen verbundenen Energien zeigen, daß zwei perfekte Zwillingszustände $\mathbf{t} = 0$ und $2\mathbf{b}_1$ stabil sind, wohingegen alle anderen Zustände metastabil sind.

1. INTRODUCTION

With few exceptions, metals and alloys are used in polycrystalline form. The boundaries between grains in these materials play a decisive role in determining their physical properties. Since internal interfaces may be regarded as anisotropic phases with a complex crystallography, many different types of grain boundary structures are possible.

In addition to the more common thermodynamic variables such as temperature, pressure and chemical potential, the excess Gibbs free energy of a crystalline interface depends on various geometrical parameters. These parameters are involved in the idealized construction of the interface. In fact, nine geometrical variables are needed to completely specify the geometrical state of a planar boundary [1]. Three angular variables specify the rigid body misorientation **R** between the two grains. Three more variables describe any relative rigid body translation **t** between the grains. The remaining three variables specify the exact orientation **n** and location, $\mathbf{n}_0$, of the plane of the interface (**n** is a unit vector normal to the boundary plane). Therefore, in its search for minimum free energy, a system containing a crystalline interface is allowed to relax any of the above parameters.

Observations of transformations of grain boundary structures such as faceting and dissociation [2] have led to the concept of grain boundary phases and grain boundary phase equilibrium diagrams. Grain boundaries are two-dimensional phases that have specific structural characteristics and free energies [3]. The unraveling of a grain boundary phase diagram with respect to varying geometrical parameters is a tremendously complicated task. In some instances, rigorous symmetry arguments, such as symmetry dictated extrema in free energy, can be useful in deriving information about the topology of interfacial phase diagrams [4, 5]. Symmetry alone, however, does not provide any information on the nature of the energy extrema.

Rigid body geometrical constructions such as the popular coincident site lattice (CSL) [6], displacement shift complete (DSC) model [7, 8] and the 0-lattice [9] have proved to be inadequate [10] for explaining low interfacial energies. Any understanding of the variation of the interfacial energy with the geometrical variables must also take into account the atomic structure and the nature of bonding at the grain boundary. The dislocation model of grain boundaries introduces some energic criterion into the description of grain boundaries [11]. For boundaries deviating from special orientations, however, the usefulness of the model is limited. The reason for this is that the interface cannot be uniquely described in terms of just primary and secondary dislocations [9].

To date, the atomic structure and interfacial energy of only a few specific grain boundaries in aluminum have been determined. With high-resolution electron microscopy (HREM), direct lattice imaging of only a few low angle grain boundaries [12, 13], a coherent twin boundary [14] and some high angle grain boundaries [15, 16] have been resolved. Moreover, only the [110] and [100] symmetrical tilt boundaries in aluminum have had their interfacial energies systematically measured [17].

By using analytical electron microscopy, Pond has given experimental evidence for the existence of two degenerate rigid body translational states of a $\Sigma 3(1\bar{2}1)$ boundary in aluminum [18]. Pond and Vitek have also introduced the concept of partial grain boundary DSC dislocations [19]. These partial dislocations separate grain boundary domains in different translational states. The Burgers vector of a partial DSC dislocation is defined as the difference between the translations and consequently is smaller than any DSC vector. Partial DSC dislocations have also been reported by these authors at junctions between inclined facets. In such a case the Burgers vector of the partial dislocation is the difference in translation of the adjoining facets.

This paper presents a study of translational states along the [112] direction of a $\Sigma 3(\bar{1}\bar{1}1)$ coherent twin grain boundary in aluminum. Observation of the core structure of a partial DSC dislocation by HREM is reported. Also demonstrated is evidence for the transformation of the twin boundary by atomic plane

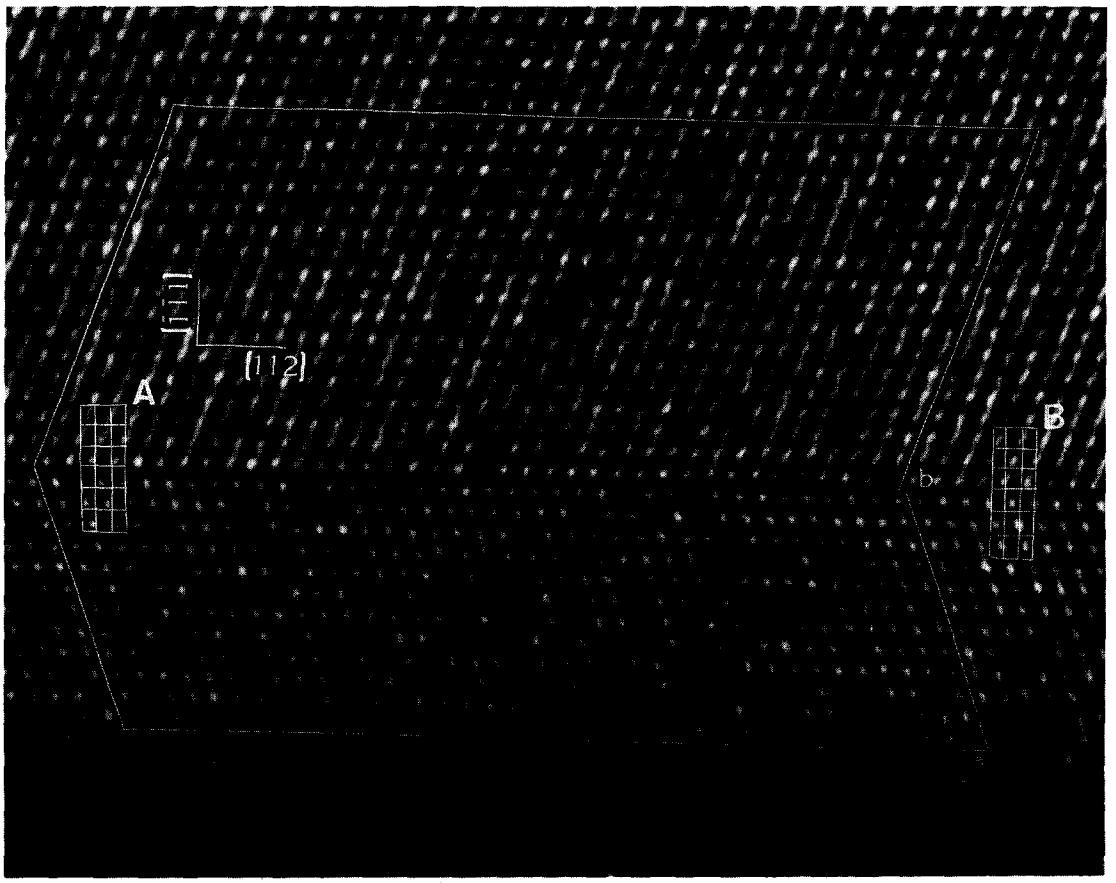

Fig. 1. HREM image of a $\Sigma 3[\bar{1}10]/(\bar{1}\bar{1}1)$ grain boundary taken near optimum defocus. The atomic columns appear black. A Frank circuit drawn around the grain boundary exhibits a closure failure of half of the DSC lattice vector $\mathbf{b}_1$, indicating the presence of a partial DSC dislocation. Two DSC lattices superposed onto the image on either side of the partial dislocation, contrast the structural difference between the $\Sigma 3$ perfect twin boundary (A), and the $\Sigma 3$ grain boundary translational state $\mathbf{t} = 1/2\ \mathbf{b}_1$ (B).

slips parallel to the boundary plane. This slipping results in boundary stepping without formation of perfect secondary DSC dislocations. Thus, the grain boundary structure is not conserved across the step. Symmetry arguments are also employed to locate symmetry dictated extrema in energy and to speculate on the topology of the bicrystal energy with respect to translation. Finally, the complete variation in energy of the boundary with rigid body translation is calculated by using a simple pair potential model. These theoretical calculations are then correlated to the experimentally observed grain boundary structures.

2. EXPERIMENTAL

The twin grain boundary was produced by heavily cold rolling a single crystal ($\sim$95% reduction) of high purity aluminum (nominal purity of 99.999%) followed by a high temperature anneal ($T \sim 500$°C). Details regarding the processing conditions can be found elsewhere [20].

For thin-foil preparation, 3 mm diameter cylindrical specimens containing these twin boundaries were trepanned from the grown samples by a spark cutting machine. The cylinders were then sliced with a diamond saw to a thickness of 0.5 mm, and ground gently on 600 grade silicon carbide paper to about 200 μm. Finally, the discs were electropolished at a voltage of 10 V at room temperature in a solution of 100 cm^3 perchloric acid and 900 cm^3 methanol diluted to 80% by glycerol. Polishing was halted just after perforation.

The thin foils thus prepared were examined with a 200 kV Hitachi electron microscope to determine angle/axis orientations of the twin boundaries. High-resolution electron microscopy was performed with a JEM-4000EX operated at 400 kV. In both electron microscopes, the specimen was usually tilted to align the direction of the electron beam with a $\langle 110 \rangle$ direction of the aluminum bicrystal. High-resolution electron micrographs were recorded near the optimum defocus typically at a magnification of 500,000 times.

3. EXPERIMENTAL RESULTS

HREM images with simultaneous lattice imaging conditions in adjacent grains of a $\Sigma 3[\bar{1}10]/(\bar{1}\bar{1}1)$ twin boundary for aluminum are shown in Figs 1, 2

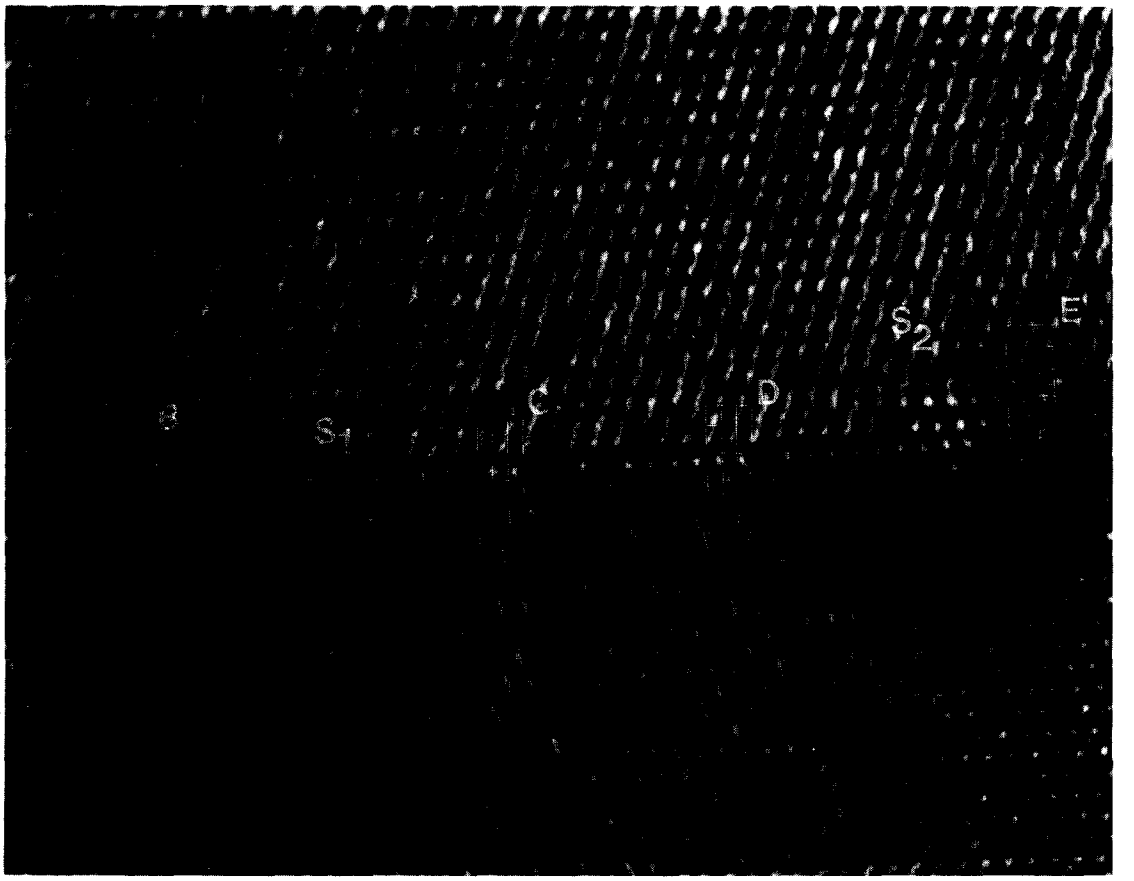

Fig. 2. HREM image of the $\Sigma 3$ bicrystal in the $\mathbf{t} = 1/2\ \mathbf{b}_1$ translational state. S_1 and S_2 indicate the location of a step and double step, respectively. The difference in grain boundary structure is best seen in the DSC lattices, B, C, D and E, superposed onto the image. See text for more details.

and 4. Each of these pictures represents successive segments of the same boundary along the [112] direction. The atomic columns appear black and the grain boundary structure is clearly resolvable.

3.1. Partial DSC dislocation

On the left side of Fig. 1, the image consists of a perfect twin boundary structure in which all atomic sites across the interface are coincident. In this region, two DSC lattice units (labelled as A) are superimposed onto the projected point pattern of the $\Sigma 3$ twin boundary. This perfect twin region of the HREM is schematically represented in Fig. 3(A). The DSC lattice vectors of the $\Sigma = 3$ misorientation are $\mathbf{b}_1 = 1/6[112]$, $\mathbf{b}_2 = 1/6[2\bar{1}1]$ and $\mathbf{b}_3 = 1/3[\bar{1}\bar{1}1]$. Both $\mathbf{b}_1$ and $\mathbf{b}_2$ are located on the twin plane, while $\mathbf{b}_3$ lies along the twin boundary normal [21].

As we move along the grain boundary plane from left to right, the (111) planes of each crystal are continuously displaced over a length of approximately 60 Å. A Frank circuit drawn around this region gives a closure failure $\mathbf{b} \sim 1/2\,\mathbf{b}_1$. This indicates the presence of a partial DSC lattice dislocation separating two translational states of the twin: $\mathbf{t} = 0$ and $\mathbf{t} = 1/2\ \mathbf{b}_1$. The structural difference between these two states is best contrasted by comparing their

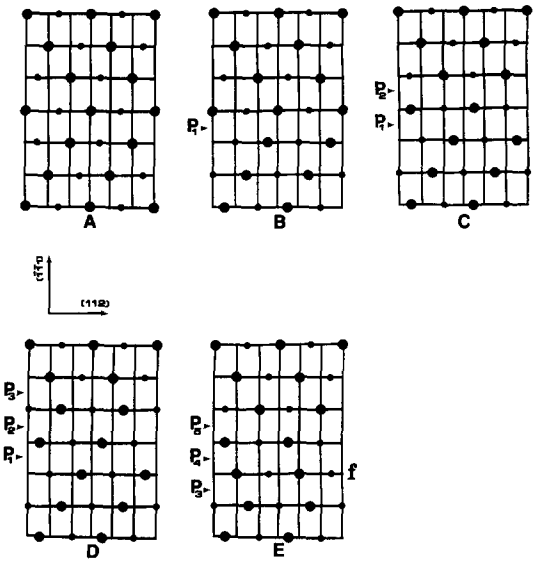

Fig. 3. Schematic representation of the grain boundary structural changes observed in the HREM images of the $\Sigma 3$ bicrystal. The large and small dots represent two successive $(\bar{1}10)$ planes. See text for details.

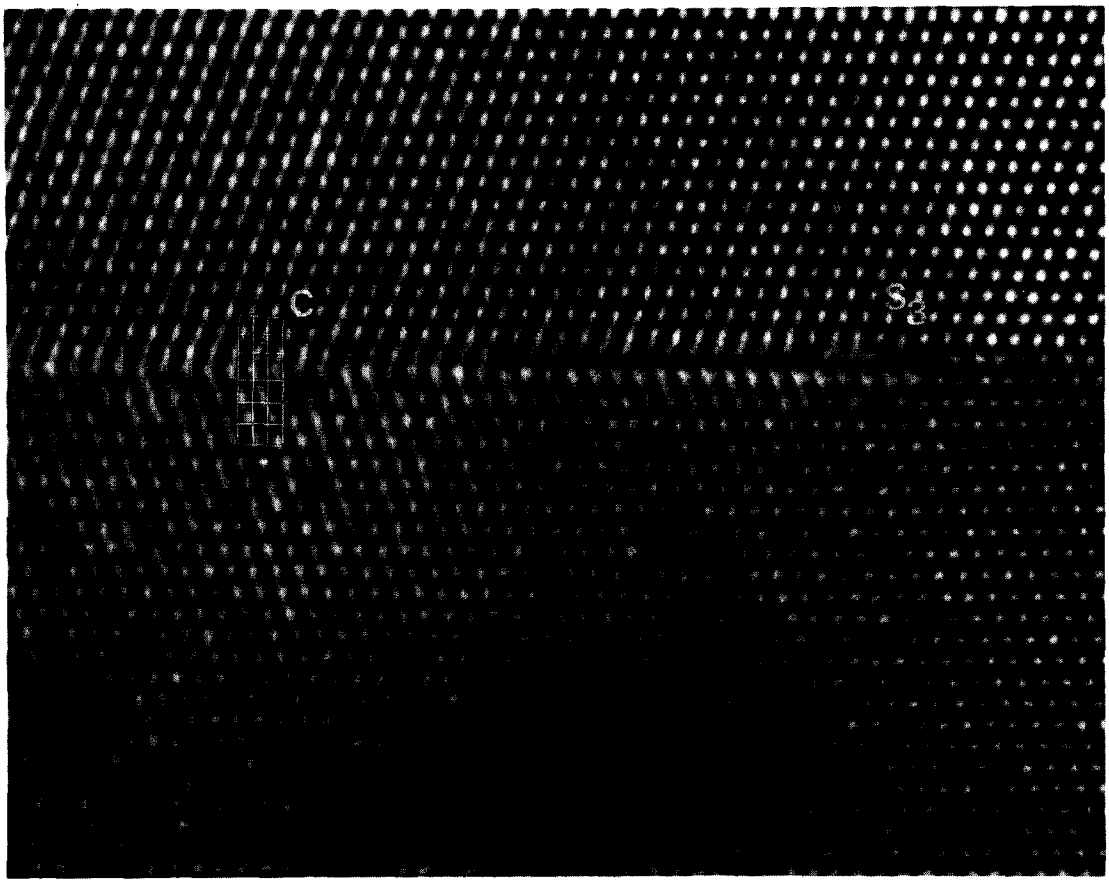

Fig. 4. HREM image of the $\Sigma 3$, $\mathbf{t} = 1/2\ \mathbf{b}_1$ bicrystal, showing the formation of a grain boundary step, S_3, by displacement along the [112] direction of atoms in a $(\bar{1}\bar{1}1)$ plane adjacent to the grain boundary.

respective DSC lattice projected patterns labelled A and B in Fig. 1 [pattern B is also depicted in Fig. 3(B)].

3.2. Grain boundary structures

Structural changes taking place further along the [112] direction are shown in the HREM pictures of Figs 2 and 4. These changes are associated with grain boundary relocations. To describe the migration of the grain boundary plane, we take plane P_1 as a reference (see Fig. 3). The first transformation in Fig. 2 is from pattern B to C. It is characterized by a relocation of the boundary plane from P_1 to P_2 as shown in Fig. 3(c). This relocation produces the single step, S_1. The next transformation is from pattern C to D, and also features a relocation of the boundary from plane P_2 to P_3 (Fig. 3D). An inspection of the image reveals additional relaxations parallel and perpendicular to the grain boundary plane. As we move further along the boundary a double step, S_2, forms. This step is characterized by a displacement of the boundary plane from P_3 to P_5 [see Fig. 3(e)].

Frank circuits drawn around steps S_1 and S_2 do in fact close, indicating the absence of grain boundary dislocations. The formation of the double step results in a fault in the stacking sequence of the $(\bar{1}\bar{1}1)$ planes of the lower crystal in the vicinity of the boundary. The faulty plane is indicated as "f" in Fig. 3(e), and is related to perfect $(\bar{1}\bar{1}1)$ stacking through a translation $1/4[\bar{1}10]$. The HREM image exhibits poor atomic column resolution in the region adjacent to the fault, which may indicate that atomic relaxation along the $[\bar{1}10]$ direction has occurred. The lower crystal seems to recover from this distortion after a few tens of Angstroms along the boundary, and the region of poor atomic contrast disappears. Figure 4 represents the structure of the twin boundary further along [112], away from the double step. On the left side of the image, atomic columns belonging to both crystals are well resolved. In the absence of any other supportive evidence, it is tentatively assumed that the fault originating at the double step has been fully relaxed here, and that the lower crystal has recovered its perfect structure. This portion of the grain boundary is structurally equivalent to Fig. 3(c).

At its right side, Fig. 4 clearly displays a continuous displacement of atoms in a single $(\bar{1}\bar{1}1)$ plane adjacent to the grain boundary. This displacement leads to a grain boundary plane relocation and gives birth to another grain boundary step labelled S_3. In fact, each of the grain boundary relocations discussed in this section can be similarly described as the result of a continuous displacement of atoms.

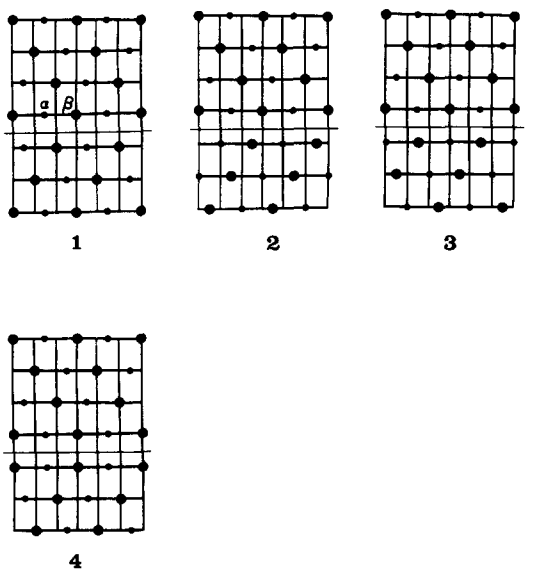

Fig. 5. $\Sigma 3$ translational states. The structures 1, 2, 3 and 4 represent the translational states $\mathbf{t} = 0$, $1/2\ \mathbf{b}_1$, $-1/2\ \mathbf{b}_1$ and $\mathbf{b}_1$, respectively. The boundary plane is represented by a thin horizontal line.

4. THEORETICAL ANALYSIS

4.1. Symmetry

In Section 3 we described the structural transformations along the $\Sigma 3$ grain boundary observed in the HREM micrographs. These transformations involve atomic displacement along the [112] direction as well as grain boundary plane relocation. A change in the boundary location, however, is equivalent to a change in the rigid body translation vector, **t**, with a fixed boundary location; therefore, the energy of the observed grain boundary structures can be understood by considering only changes in **t**. Such changes are illustrated in Fig. 5. In this figure we have taken the perfect twin as a reference state for translation (i.e. $\mathbf{t} = 0$). Ideally the grain boundary plane should reside on the twinning plane. However, since we cannot split the coincident atoms during translation, we have taken the boundary plane of translation to lie just below the twinning plane.

We have chosen to look at the translational states with some of the highest symmetry at $\mathbf{t} = \mathbf{0}$, $1/2\ \mathbf{b}_1$, $-1/2\ \mathbf{b}_1$ and $\mathbf{b}_1$. By inspection of the boundary we can determine the bicrystal symmetry. The $\mathbf{t} = 0$ and $\mathbf{t} = \mathbf{b}_1$ bicrystals (Figs 5.1 and 5.4) both have symmetry $p2'm'm$. For the $t = 1/2\ \mathbf{b}_1$ and $t = -1/2\ \mathbf{b}_1$ states (Figs 5.2 and 5.3) the symmetry is pm and $p2_1'b'm$, respectively. In Figs 5.3 and 5.4 the grain boundary plane resides on a colored mirror plane, thus these translations correspond to symmetry dictated extrema in energy. It is worth noting that our translational state $\mathbf{t} = \mathbf{b}_1$ (Fig. 5.4) is equivalent to the reference state for symmetrical tilt boundaries introduced by Pond and Bollman [22]. Curiously, the perfect twin in Fig. 5.1 does not correspond to a symmetry dictated extremum in energy. The reason for this is that the boundary plane about which the translation occurs is not located on the colored

mirror plane. To restore symmetry during translation we may introduce a nonplanar boundary. This surface may be visualized as a sinusoidal interface which alternately assigns coincident boundary atoms to the upper and lower crystals. These different atomic sites are labelled α and β in Fig. 5.1. The result is two crystals which are atomically jagged, fit together like a jigsaw puzzle. This allows translation of one grain with respect to the other about the colored mirror plane of the structure; therefore, energy varies symmetrically with translation parallel to [112]. When considering this second type of translation, another symmetry dictated extremum is found at $\mathbf{t} = 3/2\ \mathbf{b}_1$.

4.2. Energy calculations

While symmetry analysis gives the location of energy extrema, it does not provide information about the nature of the extrema. To identify an extremum as a maximum, minimum, or saddle point, energy calculations must be performed. This section reports the results of numerical calculations of potential energy for aluminum $\Sigma 3[\bar{1}10]/(\bar{1}\bar{1}1)$ bicrystals in various rigid body translational states. To determine the energy of the bicrystals, a pair potential derived from pseudopotential theory is used [23]. All calculations are carried out using a static bicrystal, disallowing atomic relaxation at the grain boundary core. In agreement with symmetry predictions, calculations show the energy varying periodically with crystal translation in the [112] direction (see Fig. 6).

The two curves plotted in Fig. 6 represent the energies resulting from two different methods of crystal translation, both in the [112] direction and both starting with a perfect twin structure. Curve (a) is generated by alternatively assigning coincident boundary atoms to the top and bottom halves of the bicrystal (the aforementioned jagged boundary). Curve (b) is generated by assigning all of the coincident atoms to only one of the two crystals, creating an asymmetric boundary. Both translation methods give identical structures at the $\mathbf{t} = 0$ perfect twin configuration, and subsequently they have the same energy value in this state.

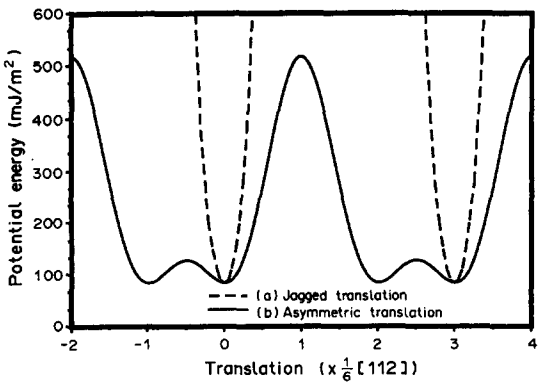

Fig. 6. Potential energy versus rigid body translation. The dashed curve (a) and continuous curve (b) correspond to translation of a jagged bicrystal and the translation of Fig. 5, respectively. Curve (a) has a maximum in energy at $\mathbf{t} = 3/2\ \mathbf{b}_1$ which is not shown in the figure.

As predicted, curve (a) contains two symmetrical extrema in energy, a minimum at $\mathbf{t} = 0$ and a maximum at $\mathbf{t} = 3/2\ \mathbf{b}_1$. The calculated minimum has a value of about 83 mJ/m^2, which agrees well with the experimental energy value for a perfect twin of 75 mJ/m^2. The maximum of curve (a) is orders of magnitude greater than that of the perfect twin. On this basis, curve (b) is taken as the most probable variation in boundary energy with rigid body translation. Curve (b) has symmetrical extrema at $\mathbf{t} = \mathbf{b}_1$ and $-1/2\ \mathbf{b}_1$, with two additional extrema at $\mathbf{t} = 0$ and $\mathbf{t} = 2\mathbf{b}_1$. From this curve we find that the energies of the translational states $\mathbf{t} = 0$, $1/2\ \mathbf{b}_1$, $-1/2\ \mathbf{b}_1$, $\mathbf{b}_1$ and $3/2\ \mathbf{b}_1$ are 83, 273, 129, 517 and 273 mJ/m^2 respectively. All of the above values correspond to a reasonable range of energies for naturally occurring grain boundaries in aluminum. Reference [24], for example, cites an average experimental measure of grain boundary energies in aluminum as 325 mJ/m^2.

The $\mathbf{t} = 1/2\ \mathbf{b}_1$ translational state bicrystal depicted in Fig. 3(e) contains a stacking fault in the $1/4[\bar{1}10]$ direction of a $(\bar{1}\bar{1}1)$ plane near the grain boundary. This fault is associated with the S_2 double step described earlier. Rigid energy calculations for this faulted bicrystal show an excess energy of about 400 mJ/m^2 as compared to an unfaulted bicrystal in the same $1/2\ \mathbf{b}_1$ translational state. As eluded to in the experimental section, relaxation within the faulted crystal may occur. If relaxed configurations are considered, the interfacial energy may be significantly reduced. Thus, while a fault in the stacking is energetically unfavorable, it is not energetically impossible.

5. CONCLUSION

This paper has presented experimental evidence for the occurrence of numerous grain boundary structures in a $\Sigma 3[\bar{1}10]/(\bar{1}\bar{1}1)$ bicrystal. The bicrystal was produced by high temperature annealing of a heavily deformed single crystal of aluminum. Two translational states, $\mathbf{t} = 0$ and $\mathbf{t} = 1/2\ \mathbf{b}_1$, have been observed by HREM. A partial grain boundary dislocation with Burgers vector $\mathbf{b} = 1/2\ \mathbf{b}_1$ separates these two nonequivalent translational states. Symmetry arguments and static numerical calculations of grain boundary energies indicate that the translational state $\mathbf{t} = 1/2\ \mathbf{b}_1$ does not correspond to a local minimum in energy; rather, it is approximately three times more energetic than the perfect twin. The occurrence of such a high energy state may be explained by the drastic processing conditions used for preparation of the bicrystal. We believe that for kinetic reasons, the recovery path followed by the deformed single crystal during the high temperature anneal may have resulted in the observed metastable translational state.

The bicrystal $\Sigma 3[\bar{1}10]/(\bar{1}\bar{1}1)$ possesses two symmetry related extrema at $\mathbf{t} = -1/2\,\mathbf{b}_1$ and $\mathbf{t} = \mathbf{b}_1$. We have found that both of these states are maxima, with the $\mathbf{t} = \mathbf{b}_1$ state approximately five times more energetic than the $\mathbf{t} = -1/2\,\mathbf{b}_1$ state. A third extremum is a minimum at the perfect twin, $\mathbf{t} = 0$. All of the calculated grain boundary static energies vary within the interval [83–517] mJ/m^2. When atomic relaxation is considered, these values may be lowered. Thus, all of the grain boundary structures that we have observed by HREM are energetically possible. Again, radical processing conditions may account for the presence of the observed high energy states.

Acknowledgements—We are grateful to Dr D. J. Smith, Center for Solid State Science at Arizona State University, for his assistance in high resolution electron microscopy. This research was supported in part by the Facility for High Resolution Electron Microscopy in the Center for Solid State Science at Arizona State University, established with support from the National Science Foundation (Grant No. DMR-86-11609). The authors also acknowledge the receipt of financial support from the U.S. Department of Energy under Contract No. DE-FG02-87ER45285.

REFERENCES

1. G. Kalonji, Ph.D. thesis, MIT, Cambridge, Mass. (1982).
2. P. J. Goodhew, T. Y. Tan and R. W. Balluffi, *Acta metall.* **26,** 557 (1978).
3. J. W. Cahn, *J. Physique*, Coll. 4, 199 (1982).
4. D. Gratias and R. Portier, *J. Physique*, Coll. 6, 43 (1982).
5. G. Kalonji, *J. Physique*, Coll. 4, 249 (1985).
6. M. L. Kronberg and F. M. Wilson, *Trans. Am. Inst. Min. Engrs* **85,** 26 (1964).
7. R. W. Balluffi, in *Interfacial Segregation*, Am. Soc. Metals, Metals Park, Ohio (1977).
8. D. A. Smith and R. C. Pond, *Int. Metals Rev.* **205,** 61 (1976).
9. W. Bollmann, *Crystal Defects and Crystalline Interfaces.* Springer, Berlin (1970).
10. A. P. Sutton and R. W. Balluffi, *Acta metall.* **35,** 2177 (1987).
11. J. P. Hirth and J. Lothe, *Theory of Dislocations.* Wiley, New York (1982).
12. A. Bourret and J. Desseaux, *Phil. Mag.* **A39,** 405 (1979).
13. M. Shamsuzzoha, P. A. Deymier and D. J. Smith, *Scripta metall.* To be published.
14. M. Shamsuzzoha, P. A. Deymier and D. J. Smith, *Phil. Mag.* To be published.
15. U. Dahmen and K. H. Westmacott, *Scipta metall.* **22,** 1673 (1988).
16. M. J. Mills, G. J. Thomas, M. S. Daw and F. Cosandey, *M.R.S. Proc.*, Fall Meeting, Boston (1989).
17. G. C. Hasson and C. Goux, *Scripta metall.* **5,** 889 (1971).
18. R. C. Pond, *Proc. R. Soc.* **A357,** 471 (1977).
19. R. C. Pond and V. Vitek, *Proc. R. Soc.* **A357,** 453 (1977).
20. M. Shamsuzzoha and P. A. Deymier, *Scripta metall mater.* **24,** 1303 (1990).
21. J. P. Hirth and R. W. Balluffi, *Acta metall.* **21,** 929 (1973).
22. R. C. Pond and W. Bollmann, *Phil. Trans. R. Soc.* **A292,** 449 (1979).
23. M. A. Ward, Ph.D. thesis, Imperial College, London (1985).
24. L. E. Murr, *International Phenomena in Metals and Alloys.* Addison-Wesley, Reading, Mass. (1975).